SPIE Vol. 3736, Bellingham, Washington, 1999 pp.430–436.

High power testing of optical components for LIGO

Sanichiro Yoshida, Alexander Gorlenko, David Tanner, and David Reitze

Physics Department, University of Florida, Gainesville, FL 32611

Justin D. Mansell

Applied Physics Department, Stanford University, Stanford, CA 94305

Efim Khazanov and Oleg Kulagin

Institue of Applied Physics, N. Novogorod, Russia

1.Introduction

The LIGO (Laser interferometer Gravitational-wave Observatory) detector [1] is a complex Fabry-Perot/Michelson interferometer designed to detect gravitational waves (GW) from astrophysical sources (Fig. 1). When a GW strikes the detector, the underlying space will be extended in one direction and contracted in the orthogonal direction. The LIGO detector is designed to detect this space-strain as a relative change in the lengths of the mutually orthogonal arms. Because this strain is much smaller than the arm length (typically 1 part in 10^{21}), each arm is in the form of an optical resonator, effectively increasing the arm length and hence its change for a given strain. The arm-length change is measured as the relative phase shift at the beam splitter. To cope with the tiny phase shift, LIGO detects it as a beat signal between a carrier frequency and a sideband frequency at the signal port (also called the dark port) of the Michelson interferometer. The sideband is generated by phase-modulating the carrier frequency; the modulation frequency is chosen so that the sideband is far off resonance with the resonators in the arms while the carrier frequency is on resonance. In this way, the phase shift associated with a relative arm-length change can be detected as amplitude modulation at the modulation frequency [2].

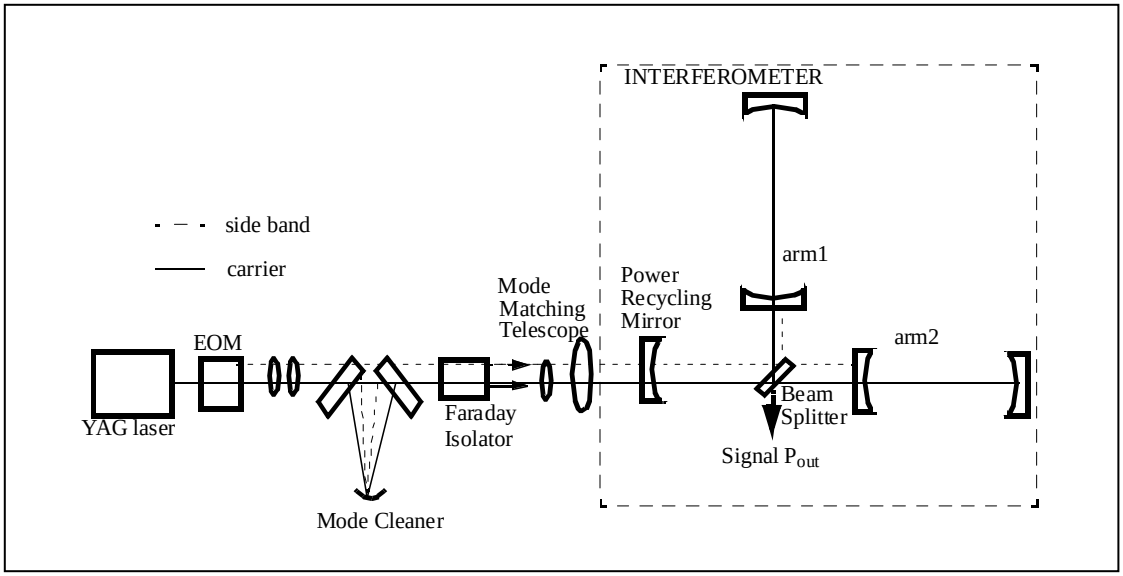

Fig. 1. The LIGO detector.

From the optical point of view, it is thus essential to mode-match the input beam to the resonators and to stabilize the beam intensity as much as possible. Note that the sensitivity of the LIGO detector is proportional to the square root of the intensity [3], and therefore it is extremely important to suppress power loss due to mode decoupling. Fig. 1 schematically illustrates the optical design of the initial LIGO detector. The output beam from a pre-stabilized, 10 W cw Nd:YAG laser is first introduced to an electro-optical modulator (EOM) for the sideband generation, and then to a mode-cleaner to eliminate all the modes except the TEM_{00} mode. Then, the beam is delivered to the interferometer through a mode-matching telescope. The Faraday isolator (FI) placed after the mode cleaner is used to isolate this mode-cleaning section from the downstream system, so that the well defined, clean input beam is not degraded by backscattering.

As is clear from the above description, the EOM and FI play important roles in the LIGO detector. In this study, we investigate the performance of these components under realistic high power conditions. The key issues for the FI are degradation of the isolation capability due to thermally-induced depolarization, and wavefront distortion caused by thermal lensing in the active medium. For the EOM, the stability of the intensity at the modulation frequency is the most important item to be examined. In this paper we present the results of our studies and discuss them in light of the requirements for the initial LIGO detector.

2.Faraday Isolator Performance

2.1. Isolation

Fig. 2 shows the optical setup we used to measure the performance of the FI. A typical FI consists of a pair of polarizers, a Faraday rotator (FR) and a half-wave plate. The FR is an opto-magnetic active medium placed in a magnetic field. The field strength and crystal length are adjusted to rotate a given linear polarization by 45° in one direction relative to the magnetic field, independent of the propagation direction the beam. Suppose the incident beam is lineally polarized in the direction vertical to the optical table. After passing through the first polarizer (polarizer 1) the polarization is rotated by the FR by 45°, and rotated back to the original vertical position by the half-wave plate. The second polarizer (polarizer 2) is aligned parallel to the first polarizer, so that it transmits the beam completely. When the beam returns from the optic placed further downstream (in Fig. 2 mirror M represents such an optic), polarizer 2 transmits the vertical component of the polarization and rejects the horizontal component by reflecting it aside. The half-wave plate rotates the polarization by 45° and this polarization is incident on the FR from the other side. Since the FR rotates the polarization of this beam in the same direction as the initial beam, the polarization becomes parallel to the optical table when it reaches polarizer 1, and is therefore rejected by it. The quality of the isolation is measured by the double-pass isolation ratio, defined as the ratio of the portion of the returning power passing through polarizer 1 to that rejected by polarizer 1.

Thus the performance of a FI is determined by how well it extinguishes the undesired polarization after a single pass, where this single-pass extinction capability (called the single-pass isolation) depends on the extinction ratio of the polarizers and the degree of depolarization in the FR. In the LIGO detector, a low single-pass isolation ratio not only degrades the isolation capability but also lowers the power delivered to the interferometer and hence the detector sensitivity. In the initial LIGO detector, the single-pass isolation ratio is required to be not less than 35 dB in intensity.

We measured the single-pass and the double-pass isolation ratios for a TGG based FR (Electro-optics TechnologiesModel 8R-1064) using a 10 W cw Nd:YAG laser (Lightwave model 220-1064-10000). The undesired portion of the polarization was measured by a photodiode (EGG model FND-100) and the desired polarization was measured by a power meter (Coherent model Fieldmaster LM10). The measurement was made using the following procedure: first with neither the FR nor the half-wave plate installed, we adjusted the direction of polarizer 1 about the beam path in such a way that the transmission might be maximized, and rotated polarizer 2 in such a way that the signal detected by the photodetector placed after polarizer 2 might be minimized. This process aligned polarizer 1 to the incident polarization and set the two polarizers orthogonal to each other. We then inserted the FR and the half-wave plate, and rotated the half-wave plate until the photodetector signal was minimized. At the same time, we measured the power reflected by polarizer 2 by the power meter. Thus the single-pass isolation was evaluated as P_{t2}/P_{r2}, where P_{t2} and P_{r2} are, respectively, the power transmitted through and reflected by polarizer 2. For the double-pass measurement, we rotated polarizer 2 by 90° about the beam path, replaced the photo-diode by a mirror of 100% reflectivity, and moved the photo-diode and the power meter, respectively, next to polarizer 1 and the optical wedge functioning as a beam splitter. Because the total single-pass rotation angle of the FR was not exactly 45°, we rotated the half-wave plate until the photodiode signal was minimized. The double-pass isolation ratio was then evaluated as P_{t1}/P_{r1}, where P_{t1} and P_{r1} are the power transmitted through and reflected by polarizer 2.

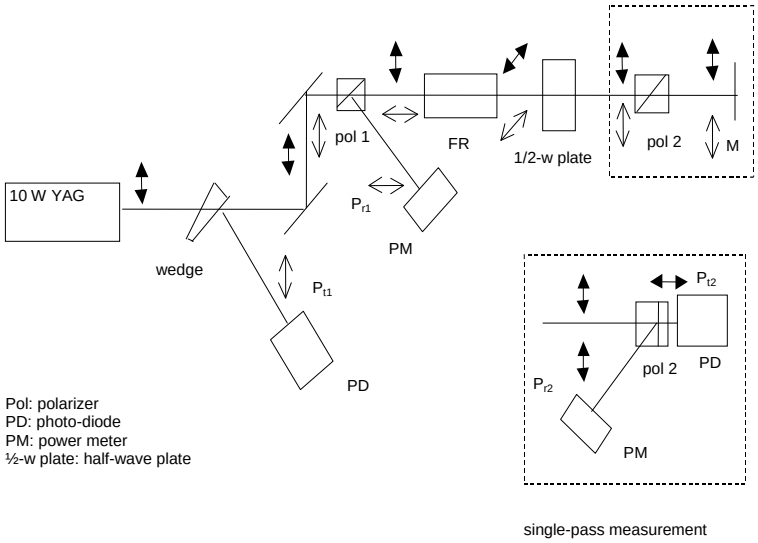

Fig. 2. Measurement of isolation ratio. Thick arrows denote polarizations of the ongoing beam and thin arrows denote those of the returning beam.

Fig. 3 shows the results of these measurements as a function of laser power transmitted through the FR. The double-pass isolation and the single-pass isolation coincide with each other, showing a slight dependence on the laser power. In the whole laser power range, the isolation ratio was a factor of two lower than the required level of 35 dB.

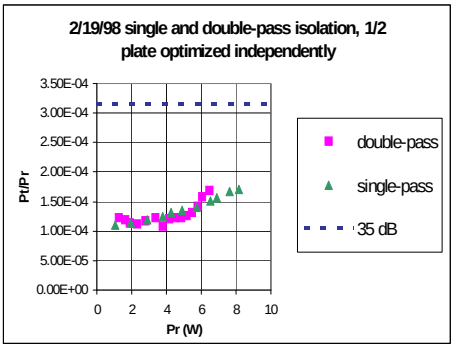

Fig. 3 Isolation ratio

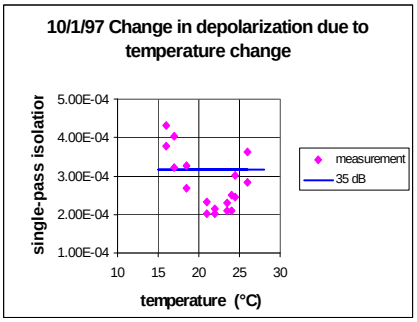

Fig. 4 Temperature dependence of single-pass isolation

Because the Verdet constant of the TGG crystal depends on the temperature, the total angle of the Faraday rotation is dependent on the temperature. This dependence means that if the ambient temperature varies after the direction of the half-wave plate is adjusted, the isolation will be degraded because the resultant polarization is not aligned with polarizer 2. To examine this effect, we deliberately varied the ambient temperature and measured the change in the single-pass isolation. The result is shown in Fig. 4. When the temperature change is more than 3°C, the isolation was degraded beyond the required value of 35 dB.

2.2. Thermal lensing

When a laser heats a transmissive optic, a temperature distribution is established over the cross section of the beam, causing a radial distribution of the optical path length. Consequently, the optic behaves as if it is a lens; this effect is called thermal lensing. In this part of our study, we measured the thermal lensing in the FR using a Shack-Hartmann wavefront detector [4] (SHWD, Wavefront Sciences model 285336). Fig. 5 illustrates the experimental arrangement. We employed a pump-and-probe arrangement using a He/Ne laser (Melles Griot, model 05-LLR-811-249) as the probe laser. The reasons for this

arrangement are (i) the SHWD is higher in sensitivity at 633 nm than at 1.06 μm and (ii) power balancing to ensure constant intensity on the SHWD is not necessary as the pump beam power is varied. The pumping laser was the same Nd:YAG laser shown in Fig. 2. The probe laser beam was introduced into the FR collinearly with the pump beam. M2 and M3 are dichroic mirrors that pass the probe laser and reflect the pump laser. A power meter measured the pump beam power transmitted through the FR. The thermal lensing was evaluated by comparing the wavefront detected by the SHWD at various pump-beam powers with a common reference wavefront that was taken with the pump beam off and the other optics unchanged.

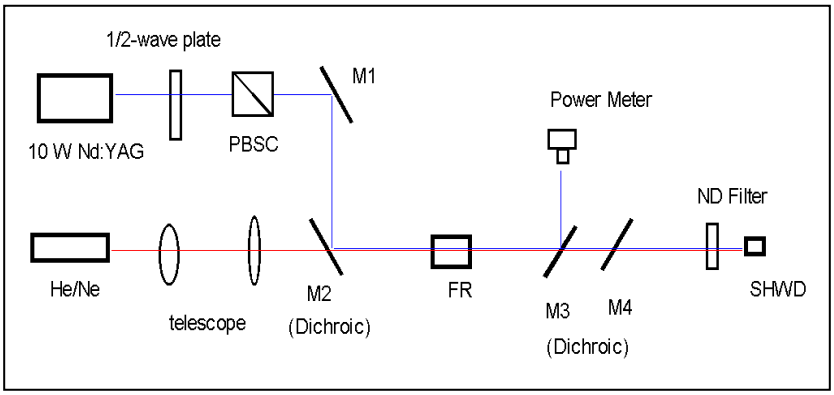

Fig. 5. Measurement of thermal lensing.

Fig. 6 shows the thermal lensing observed at pumping powers of 7.7 W and 3.9 W. The waist size of the pump beam was measured to be 1.37 mm at the location of the FR. In the case of a TGG crystal, the dominant mechanisms of thermal lensing are the variation of the refractive index due to the temperature change (*dn/dT*) and due to longitudinal thermal expansion.

$$\Delta OPL(r) = (\frac{dn}{dT} + \alpha n) L \Delta T(r) \tag{1}$$

where ΔOPL is the optical path change, L is the crystal length, α is the thermal expansion coefficient, n is the refractive index and $\Delta T(r)$ is the temperature distribution over the beam cross section. Strain et al.[5] have shown that when a cylindrical substrate is heated by a Gaussian laser beam whose waist size is much smaller than the substrate's radius the resultant temperature rise can be expressed by the following polynomial.

$$\Delta T(r) = (\frac{P \gamma_{ab}}{4\pi\kappa}) \sum_{k=1}^{\infty} (2\frac{r^2}{w^2})^k \frac{(-1)^k}{kk!} \tag{2}$$

where P is the laser power, γ_{ab} is the absorption coefficient, w is the waist size, κ is the thermal conductivity and k is an integer representing the order of the polynomial. Using the above formulas and the numbers shown in the table below, we calculated theoretical $\Delta OPL(r)$ and compare with the measurement in Fig. 6. Good agreement is seen between the measurement and the calculation.

κ (W/m k)	dn/dT (1/K)	n	TGG length (cm)	γ_{ab} (1/cm)	α (1/K)
7.4	2 x 10^{-5}	1.95	2	1x 10^{-3}	9.4 x 10^{-6}

In Fig. 7, ΔOPL measured at the pump beam waist is plotted as a function of the pump beam power. Extrapolation of this plot indicates that ΔOPL at 10 W is about 18 nm. This value corresponds to an effective focal length of 53 m. Here the effective foal length was evaluated by fitting the measured thermal lens to $\Delta OPL = r^2/2F$, where r is the radial distance from

the thermal-lens-center and *F* is the effective focal length of the thermal lens. According to our mode coupling calculation, the power coupling loss due to this thermal lens is less than 1%.

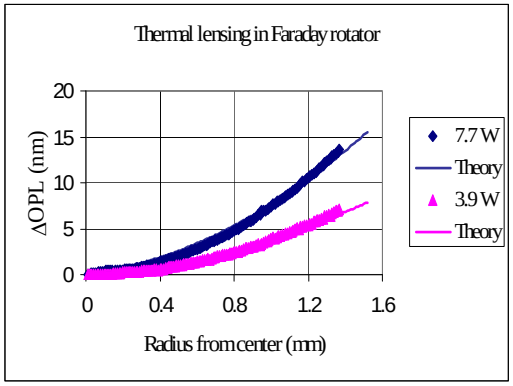

Fig. 6. Thermal lensing in the FR.

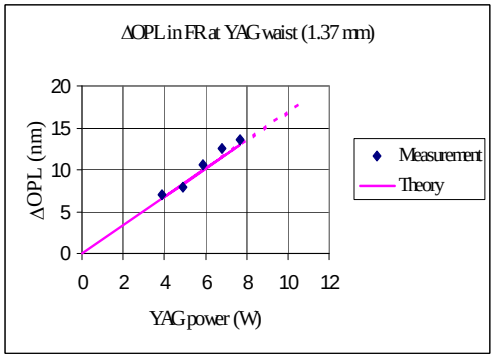

Fig. 7. Thermally induced optical path change at YAG waist.

3.Electro-optical Modulator Performance

In the LIGO detector the EOM is expected to function as a pure phase modulator. In reality, however, unavoidable misalignment among the directions of the incident polarization, the EOM's axis and the orientation of the polarizer causes some degree of intensity modulation [6] (called the residual intensity modulation). Fig. 8 illustrates such a situation where the initial polarization and the polarizer have angular misalignments of β and γ, respectively.

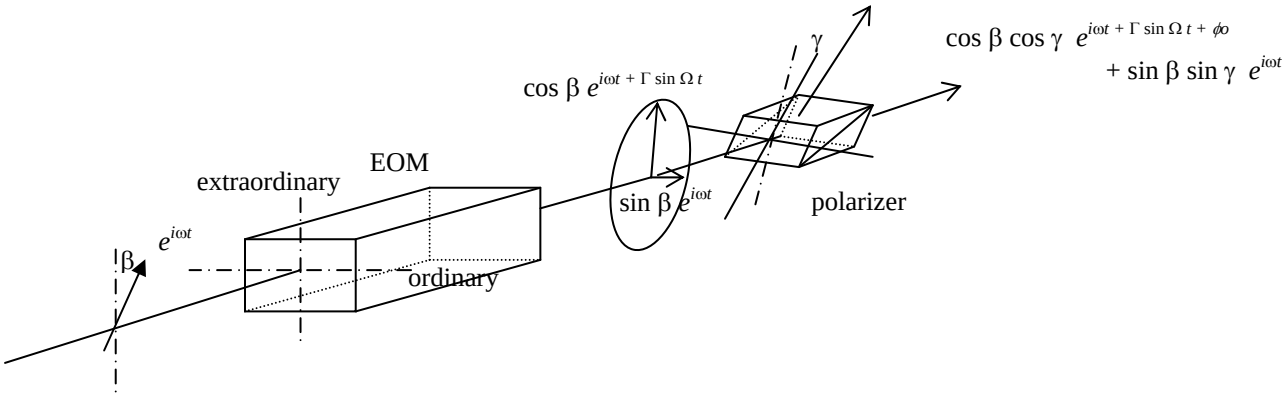

Fig. 8. Residual intensity modulation caused by angular misalignment.

In this situation, the intensity of the light transmitted through the polarizer can be expressed as follows.

$$T = \cos^2\beta \cdot \cos^2\gamma + \sin^2\beta \cdot \sin^2\gamma + 2\cos\beta \cdot \cos\gamma \cdot \sin\beta \cdot \sin\gamma \cdot \cos(\Gamma \sin\Omega t + \phi_0) \tag{3}$$

Here ϕ_0 is the initial phase retardation in the EOM, Ω is the phase modulation frequency, and Γ is the modulation index. As seen in this equation, the residual intensity modulation occurs at the phase modulation frequency Ω, and therefore can affect the gravitational wave signal. The initial LIGO requires the level of the residual intensity modulation to be not greater than 10^{-3}. We measured the intensity modulation under realistic conditions to see if this requirement can be met.

Fig. 9 illustrates the arrangement for this measurement. A $LiNbO_3$-based EOM (New Focus, Inc. model 4003) was driven at 21 MHz and the 10 W Nd:YAG laser was focused through the EOM to heat the $LiNbO_3$ crystal. The waist size of the 10 W Nd:YAG laser at the EOM was measured to be less than 0.4 mm. This power density is higher than the value expected in the initial LIGO detector. Because this Nd:YAG laser oscillates in multiple longitudinal modes, it is not suitable for the sideband spectrum analysis. Therefore, we used a single mode Nd:YAG laser (Lightwave model 220-1064-7000) as a probe laser. In order to separate the probe laser beam from the heating beam, we arranged the polarization of the probe beam orthogonal to the heating beam. Thus two cubic polarizers were placed orthogonal to each other as shown in Fig. 9, so that both beams would merge at the first polarizer and the probe laser would pass through the second polarizer while the heating beam would be reflected by the second polarizer. The reflected beam was used to monitor the transmitted power level. The probe Nd:YAG beam transmitted through the second cubic polarizer was detected by an RF photodiode (EGG model FND-100) whose output was fed to an RF spectrum analyzer (RFSA. Hewlett Packard model 8557A) and an oscilloscope. The former was used to measure the RF component (called the ac component) and the latter was used to measure the average power (called the dc component). A neutral density filter was used to reduce the power level when the ac component was measured by the RFSA.

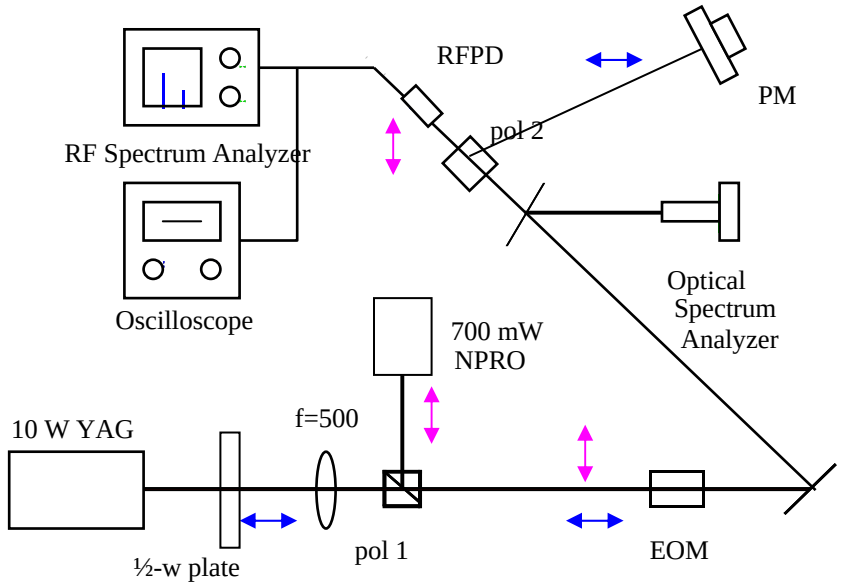

Fig. 9. Measurement of depolarization and intensity modulation in EOM.

The measurement was made using a modulation index Γ=0.4, a realistic value for the LIGO detector. Fig. 10 shows the residual intensity observed at the heating power level of 10 W and its temporal variation. For more than two hours, the residual intensity stayed lower than 10^{-6}, which is lower than the above-mentioned requirement by more than three orders of magnitude. Slight change observed around t=90 min is considered to be caused by the change in the transmission T due to a temperature change that causes a change in the initial retardation ϕ_0. Since $LiNbO_3$ has higher dn/dT for the extraordinary ray than for the ordinary ray, and because the EOM uses the extraordinary ray for the phase modulation, a temperature change causes the initial retardation ϕ_0 to be changed. Because the sensitivity of the cosine function depends on the phase, the cos (Γ sin $\Omega t + \phi_0$) term varies if ϕ_0 changes.

In Fig. 11, the dependence of the residual intensity on the heating power is shown. When the heating power is varied, the $LiNbO_3$ crystal's also changes. In turn, the transmission changes, for the same reason mentioned in the preceding paragraph. However, at all the powers examined, the residual intensity modulation is lower than 10^{-6} and no substantial power dependence is observed. This result indicates that, except for the slight temperature change, the power level in this power range is not the issue for the residual intensity modulation.

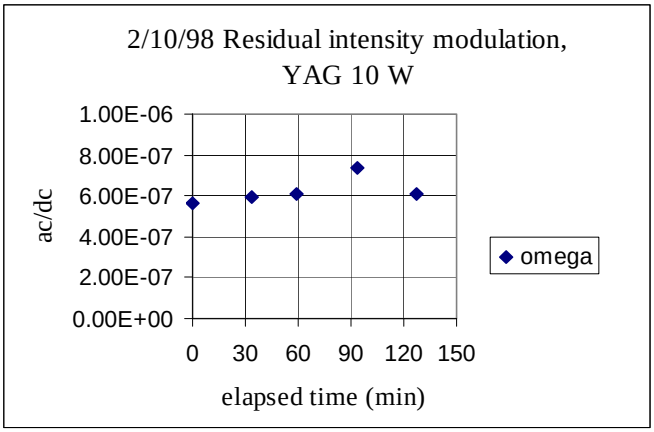

Fig. 10. Residual intensity modulation. The modulation depth=0.4.

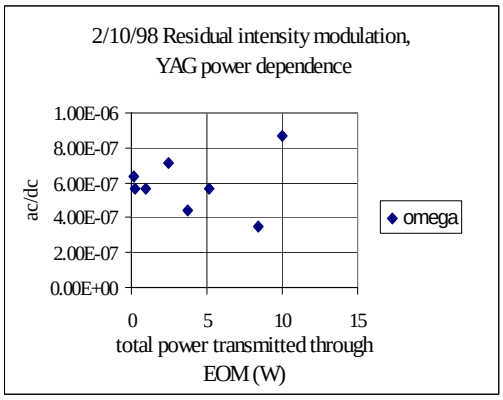

Fig. 11. Residual intensity at various pump powers.

4.Conclusions

In summary, we evaluated the performance of a TGG-based Faraday isolator and a $LiNbO_3$-based electro-optic phase modulator under high power conditions realistic for the initial LIGO detector. At a power level of 8 W, the Faraday isolator showed an isolation ratio of 38 dB. The performance is about 50% worse than at the power level of 1 W, but still better than the requirement by a factor of two. The thermal lensing observed in the Faraday rotator at the power level of 8 W was 13.5 nm in the optical path difference over the YAG laser's waist size. This optical path difference is equivalent to an effective focal length of 53 m, which corresponds to power decoupling loss of less than 1% and which is compensatable by the mode-matching telescope. The electro-optic modulator showed residual intensity modulation at a level lower than 10^{-6}, which is three orders of magnitude lower than the requirement. The observed residual intensity modulation depended neither on the YAG laser power nor on the time the modulator was exposed to the high power.

5. Acknowledgements

The authors gratefully acknowledge the National Science Foundation (grant PHY-9722114) in financial support of this research.

6. References

1. A. Abramovici et al., Science, 256, 325 – 333 (1992)
2. P. Saulson, *Fundamentals of Interferometric Gravitational Wave Detectors* (World Scientific, Singapore, New Jersey, London, Hong Kong, 1994) p.203 – 206.
3. P. Saulson, *Fundamentals of Interferometric Gravitational Wave Detectors* (World Scientific, Singapore, New Jersey, London, Hong Kong, 1994) p.199.
4. D. R. Neal, D. J. Armstrong and W. T. Turner, "Wavefront sensors for control and process monitoring in optics manufacture, SPIE 2993-29, 1-10 (1997)
5. K.A. Strain, K. Danzmann, J. Mizuno, P.G. Nelson, A. Rüdiger, R. Schilling and W. Winkler, "Thermal lensing in recycling interferometric gravitational wave detectors", Phys. Lett. A, 194, 124-132 (1994)
6. S. Kawamura, A. Abramovici and M. E. Zucker, "Improved multistage wide band laser frequency stabilization," Rev. Sci. Inst., 68, 223-229 (1997)